Journal of Materials Chemistry B

ROYAL SOCIETY OF CHEMISTRY

PAPER

View Article Online
View Journal | View Issue

Cite this: *J. Mater. Chem. B*, 2021, **9**, 3168

Cytochrome *C* with peroxidase-like activity encapsulated inside the small DPS protein nanocage†

Hitesh Kumar Waghwani and Trevor Douglas *

Nature utilizes self-assembled protein-based structures as subcellular compartments in prokaryotes to sequester catalysts for specialized biochemical reactions. These protein cage structures provide unique isolated environments for the encapsulated enzymes. Understanding these systems is useful in the bioinspired design of synthetic catalytic organelle-like nanomaterials. The DNA binding protein from starved cells (Dps), isolated from *Sulfolobus solfataricus*, is a 9 nm dodecameric protein cage making it the smallest known naturally occurring protein cage. It is naturally over-expressed in response to oxidative stress. The small size, natural biodistribution to the kidney, and ability to cross the glomerular filtration barrier in *in vivo* experiments highlight its potential as a synthetic antioxidant. Cytochrome *C* (CytC) is a small heme protein with peroxidase-like activity involved in the electron transport chain and also plays a critical role in cellular apoptosis. Here we report the encapsulation of CytC inside the 5 nm interior cavity of Dps and demonstrate the catalytic activity of the resultant Dps nanocage with enhanced antioxidant behavior. The small cavity can accommodate a single CytC and this was achieved through self-assembly of chimeric cages comprising Dps subunits and a Dps subunit to which the CytC was fused. For selective isolation of CytC containing Dps cages, we utilized engineered polyhistidine tag present only on the enzyme fused Dps subunits (6His-Dps-CytC). The catalytic activity of encapsulated CytC was studied using guaiacol and 3,3′,5,5′-tetramethylbenzidine (TMB) as two different peroxidase substrates and compared to the free (unencapsulated) CytC activity. The encapsulated CytC showed better pH dependent catalytic activity compared to free enzyme and provides a proof-of-concept model to engineer these small protein cages for their potential as catalytic nanoreactors.

Received 4th February 2021,
Accepted 16th March 2021

DOI: 10.1039/d1tb00234a

rsc.li/materials-b

Introduction

Cells are hierarchically organized structures comprising many subcellular compartments that segregate macromolecules and biochemical reactions from the rest of the cell.[1,2] They utilize lipid and/or protein-based organelles to co-localize and protect enzymes and co-factors, separate reactive intermediates from other cellular components and provide unique isolated micro-environments.[3] Peroxisomes, for example, contain oxidase and catalase enzymes that are involved in the formation and scavenging of hydrogen peroxide whereas acidocalcisomes accomplish calcium sequestration with the help of a phosphate rich acidic lumen and a pH gradient across its membrane.[3,4] Unlike eukaryotes, prokaryotes possess subcellular organelles assembled from proteins that are able to catalyze unique and specific biochemical reactions by co-encapsulation of sequential enzymes and co-factors.[5] Understanding of these systems has generated significant interest in the design and synthesis of artificial micro and nano-compartments as functional biomimetic materials.[6–12] To mimic the complex cellular functions and create synthetic cell-like nanomaterials, it is important to understand the reactions that take place inside subcellular compartments at the molecular level.

Protein-based architectures, which assemble into cage-like structures, such as the carboxysomes, house multiple enzymes responsible for carbon fixation in some bacteria, while encapsulins from *Thermotoga maritima* mediate oxidative stress response through encapsulated peroxidases.[13–15] While protein cages often self-assemble from a limited number of identical subunits into highly symmetrical structures, the presence of chimeric cage structures has also been observed naturally. The 24-subunit cages comprising mammalian ferritins are naturally occurring chimeric cage structures composed of different proportions of both heavy (H) chain and light (L) subunits. The H subunits provide a catalytic center for Fe(II) oxidation whereas

Department of Chemistry, Indiana University, 800 E Kirkwood Ave., Bloomington, Indiana 47405, USA. E-mail: trevdoug@indiana.edu

† Electronic supplementary information (ESI) available. See DOI: 10.1039/d1tb00234a

L subunits are involved in iron oxide mineral core stability.[16,17] Inspired by the chimeric mammalian ferritin cages, a combination of genetic and chemical modifications was previously demonstrated in creating chimeric Dps cages with multiple chemical functionality present on both the interior and exterior of the cage.[18] Also, using a combination of computational and genetic approaches adeno-associated virus (AAV) chimera were designed for tunable gene delivery.[19,20] Here we report the design and formation of chimeric Dps cages, which encapsulate active cytochrome *C* (CytC) with peroxidase-like activity using the self-assembly of 6His-Dps-CytC fusions together with unmodified Dps subunits.

Dps (DNA binding protein from starved cells), is the smallest known protein cage with a 9 nm external diameter and 5 nm inner cavity.[21–23] The Dps we selected, isolated originally from the hyperthermophilic archaeon *Sulfolobus solfataricus*, is actively upregulated in response to oxidative stress, displays catalase activity, and plays an important role in iron homeostasis and iron oxide mineralization.[21–23] *In vivo* biodistribution studies show that Dps naturally localizes to the kidney and this has been reported to protect kidney from endotoxin-induced injury.[24] Here we explored the design and synthesis of Dps cages encapsulating CytC as cargo for its potential enhanced antioxidant activity. Cytochrome *C* (CytC) is a small 12 kDa hemoprotein, with peroxidase-like activity, involved in electron transport reactions during respiration and plays critical role in apoptosis.[25,26] The hydrodynamic diameter of CytC is ~3.4 nm which is slightly smaller than interior cavity of Dps. Encapsulation of CytC in the limited volume of Dps would provide highly crowded and confined environment for CytC and the positively charged CytC exterior surface would facilitate encapsulation within the negatively charged Dps interior cavity during self-assembly.

Here we report a novel method for peroxidase-like protein encapsulation inside the small Dps protein cage using a chimeric assembly approach. Dps subunits modified with an N-terminal polyhistidine tag and a C-terminal CytC fusion (6His-Dps-CytC) were simultaneously co-expressed with unmodified Dps subunits resulting in assembly of DpsCytC chimeric cages encapsulating CytC. The engineered polyhistidine tag facilitated the selective purification of CytC encapsulated Dps cages. The purified DpsCytC chimeric cages were catalytically active and showed different pH dependent turnovers compared to free recombinant CytC (rCytC) control expressed under similar conditions. The concentration of CytC encapsulated inside Dps was approximately 25 mM and the enzyme, under these conditions of high molar confinement, showed better catalytic turnover compared to free rCytC. In addition, using fluorescence labelling we demonstrate that the pH environment inside Dps is ~1.2 unit more basic than bulk solution which could affect the encapsulated CytC activity. Previous studies on other protein cage architectures have identified unique pH environments on the interior of bacteriophage PP7 capsids and cowpea chlorotic mottle virus (CCMV) capsids compared to the bulk solution.[27,28] This highlights the potential importance of the unique microenvironment provided by protein cage compartments as models for tunable catalytic activity of an encapsulated catalyst.

Experimental

Materials

E. cloni® EXPRESS BL21(DE3) electrocompetent cells were purchased from Lucigen (Middleton, WI). DNase, RNase, lysozyme, guaiacol, 3,3′,5,5′-tetramethylbenzidine (TMB), SYPRO orange protein gel stain and cytochrome *C* form bovine heart (12 327 Da ≥ 95%) were purchased from Sigma-Aldrich. δ-Amino levulinic acid hydrochloride was purchased from frontier scientific. H_2O_2 (50%), fluorescein-5-maleimide (F5M) and all other chemical and reagents were purchased from Thermo Fisher Scientific (Waltham, MA).

Dps C126S, C101S site directed mutagenesis

The wtDps contains two cysteine residues that we removed to avoid potential interaction with the heme of the encapsulated CytC[29,30] Using a previously prepared Dps C126S construct[31] the second exposed cysteine was replaced with serine (C101S), to generate the double cys mutant C126S, C101S, by site directed mutagenesis using 5′-atacgcatcggagctagctgaaatatcagcaagct-3′ and 5′-agcttgctgatatttca gctagctccgatgcgtat-3′ primers. The DNA sequence was verified for inserted mutation and the vector was transformed into BL21 (DE3) cells for protein expression. This protein referred here as unmodified Dps was characterized for maintenance of cage structure after point mutation by TEM and DLS (Fig. S1, ESI†) and was further used in the three-vector co-expression approach to make DpsCytC chimeric cages.

Dps-E158C site directed mutagenesis

The Dps C101S C126S protein prepared above was further engineered with a reactive cysteine (located on the interior of the Dps cage) at position 158 by single point mutation (E158C) using 5′-ctctaagaaccacgcttcgtggcatatctcttcttgaagtatcctct-3′ and 5′-agaggatacttcaagaagagatatgccacgaagcgtggttcttagag-3′ primers.

Cloning of 6His-Dps-CytC in pCDFDuet-1 vector

The codon optimized 6His-Dps-CytC gene was ordered from IDT. The plasmid for pCDFDuet-1 vector was linearized using 5′-gatccgaattcgagctcggcg-3′ and 3′-ctggctgtggtgatgatggtgatg-5′ primers and gene for 6His-Dps-CytC was cloned into pCDFDuet-1 vector using Gibson assembly. The Gibson assembly was carried out using HiFi DNA assembly master mix. After verifying the DNA sequence, the assembled vector was transformed into BL21 (DE3) cells for protein expression. A 15 amino acids linker (GAAGENLYFQSGAAG) was included as TEV protease recognition sequence between Dps and CytC.

Protein expression

For simultaneous co-expression of Dps and 6His-Dps-CytC in presence of cytochrome *C* maturation gene (*ccm* gene), a three-vector approach was used. The pCDF-Duet-1 vector (streptomycin resistance) with 6His-Dps-CytC gene, pET-30(a) vector (kanamycin resistance) with Dps C101S C126S gene and pEC86 vector

(chloramphenicol resistance) with *ccm* gene were co-transformed into BL21 (DE3) *E. coli* cells. The cells were plated on a LB-agar plate supplemented with 50 μg mL^{-1} streptomycin, 30 μg mL^{-1} kanamycin and 34 μg mL^{-1} chloramphenicol (in ethanol) to select *E. coli* colonies with all three vectors, and the plate was incubated at 37 °C overnight. One colony was picked and grown in the 2×-YT medium at 30 °C overnight in the presence of three antibiotics to maintain selection for three plasmids. The expression of Dps and 6His-Dps-CytC was induced when the o.d. at 600 nm reached 0.7 with isopropyl β-D-thiogalactopyranoside (IPTG) to a final concentration of 100 μM and δ-amino levulinic acid hydrochloride was also added as heme precursor to a final concentration of 0.5 mM. The culture was grown for an additional 24 hours at 22 °C and cells were harvested by centrifugation (4500*g* for 20 min), and cell pellets (reddish pink colored) were used freshly or stored temporarily in refrigerator for a day until further use.

A two-vector approach was used to recombinantly overexpress free cytochrome *C*. The pCDF-Duet-1 vector (streptomycin resistance) with cytochrome *C* gene and pEC86 vector (chloramphenicol resistance) with *ccm* gene were co-transformed into BL21 (DE3) *E. coli* cells. The cells were plated on a LB-agar plate supplemented with 50 μg mL^{-1} streptomycin and 34 μg mL^{-1} chloramphenicol (in ethanol) to select *E. coli* colonies with two vectors, and the plate was incubated at 37 °C overnight. A similar culture growth protocol was further followed as described above for DpsCytC.

Protein purification

DpsCytC chimeric cages. Cell pellets were resuspended in 50 mM sodium phosphate 100 mM sodium chloride pH 7.0 buffer. DNase, RNase, and lysozyme were added to final concentrations of 60, 100, and 50 μg mL^{-1}, respectively. The cell suspension was incubated for 30 min at room temperature with gentle shaking. Cells were lysed by sonication for 2 min at 50% amplitude on ice. The cell debris was separated by centrifugation (12 000*g*, 45 min, 4 °C) and the cell lysate was syringe filtered (0.45 μm) and loaded on 5 mL Roche Ni-NTA column at flow rate of 1 mL min^{-1}. The column was washed with buffer (50 mM sodium phosphate pH 7.8 with 100 mM sodium chloride and 10 mM imidazole) to remove non-specifically bound proteins and then DpsCytC chimeric cages were eluted using an imidazole gradient (10–500 mM). The elution was monitored at 280 nm (for protein) and 410 nm (for heme). Presence of Dps and 6His-Dps-CytC subunits in chimeric cages was determined by SDS-PAGE analysis. Protein fractions were combined and additionally purified over Superose 6 prep grade size-exclusion column (GE Healthcare Life Sciences) using FPLC at 0.5 mL min^{-1} flow rate with 20 mM sodium phosphate 10 mM citrate combination buffer pH 6.25. Protein elution was monitored at 280 and heme at 410 nm respectively. Protein fractions corresponding to presence of heme were combined and stored at 4 °C.

rCytC. Cell pellets were resuspended in 20 mM sodium phosphate 500 mM sodium chloride pH 6.5 buffer. DNase, RNase, and lysozyme were added to final concentrations of 60, 100, and 50 μg mL^{-1}, respectively. The cell suspension was incubated for 30 min at room temperature with gentle shaking. Cells were lysed by sonication for 2 min at 50% amplitude on ice. The cell debris was separated from the cell lysate by centrifugation (12 000g, 45 min, 4 °C) and the cell lysate was dialyzed overnight in 20 mM sodium phosphate 20 mM sodium chloride pH 6.5 buffer (Buffer A). Dialyzed protein was syringe filtered (0.22 μm) and loaded on HiTrap SP HP cation exchange chromatography (GE Healthcare) column using 20 mM sodium phosphate buffer pH 6.5 with the 0–1 M sodium chloride gradient. Fractions containing rCytC protein were further SEC purified in similar way as described above for DpsCytC chimeric cages and stored at 4 °C.

wtDps, Dps C101S C126S (Dps), DpsCytC (passively encapsulated) & Dps-E158C were recombinantly expressed in *E. coli* and purified using previously described procedures for Dps.[24]

Size-exclusion chromatography coupled with multiangle light scattering (SEC-MALS)

The molecular weights for samples were analyzed by multiangle light scattering (MALS:DAWN8$^+$, Wyatt Technology, Santa Barbara, CA) equipped with a He–Ne laser source, quasi-elastic light scattering detector, and refractive index (RI) detector (Optilab T-rEX, Wyatt Technology), which is coupled with an Agilent 1200 HPLC system. All Dps variant samples (10 mg mL^{-1}) were separated over a WTC-0100S (Wyatt Technologies) size-exclusion column at the flow rate of 0.7 mL min^{-1} of MALS buffer (50 mM sodium phosphate, 100 mM sodium chloride, 200 ppm sodium azide pH 7.2). A 25 μL sample was injected and loaded on a column. The eluted protein peaks were detected using a UV-vis detector (Agilent), a Wyatt HELEOS II multiangle laser light scattering (MALS) detector, and an Optilab rEX differential refractometer. The number-average particle molecular weight was measured across each protein peak using Astra 6.0.3.16 software (Wyatt Technologies Corporation). A refractive index increment (dn/dc) of protein (0.185) was used to calculate the molecular weight of the samples. The average molecular weight (M_W) contribution from CytC enzyme was determined by subtracting M_W of Dps empty cage ($\sim$260 kDa) from DpsCytC chimeric cage samples.

SDS-PAGE gel electrophoresis

Protein samples were mixed with the 4× SDS-PAGE loading buffer (containing 100 mM DTT final concentration) and heated in a boiling water bath for 10 min. Samples were spun on a benchtop centrifuge and separated on a 12 or 15% acrylamide gel at a constant current of 36 mA for approximately 1 h. Gels were stained with InstantBlue protein stain (Expedeon) and rinsed with water before imaging. The gel image was recorded on a UVP MultiDoc-IT digital imaging system. A 10–180 kDa PageRuler prestained protein ladder (Thermo Scientific) or 10–250 kDa Precision Plus Protein™ Standards (BIO-RAD) was used as a protein marker.

Densitometry

Densitometry analysis of SDS-PAGE gel was used to determine the relative subunit ratios of 6His-Dps-CytC and Dps in the DpsCytC chimeric cage sample. Briefly, 10 μL protein samples were applied and separated on a 12% SDS-PAGE gel. The line scan profiles of DpsCytC and Dps protein bands were obtained

using Fiji software and fitted with multipeak Gaussian fit function using Igor Pro 6.37 to obtain peak areas. The ratio of peak area of 6His-Dps-CytC to Dps was used to estimate the number of CytC encapsulated inside the chimeric cage.

Transmission electron microscopy (TEM)

Protein samples (5 μL, 0.025 mg mL^{-1}) were applied to 400 mesh carbon-coated copper grids and incubated for 2 min. Excess liquid was wicked away with a filter paper. The sample grid was then washed with 5 μL of distilled water to remove salts and stained with 5 μL of 2% uranyl acetate for 2 min. Excess stain was wicked away using the filter paper. Images were taken on a JEOL 1010 transmission electron microscope at an accelerating voltage of 80 kV. The contrast of TEM images was enhanced in Fiji software[32] for clarity.

Dynamic light scattering (DLS)

The hydrodynamic radius (R_h) of protein samples was measured by dynamic light scattering (DLS) (Zetasizer Nano-S; Malvern Instruments, Worcestershire, U.K.). Protein samples were spun in a benchtop centrifuge (12 000 rpm, 10 min) to remove any aggregates. The DLS of each sample (100 μL, 1 mg mL^{-1}) was measured in a quartz cuvette (Hellma Analytics, ZEN2112). To test the concentration dependent aggregation of free CytC, CytC_sigma was solubilized in 50 mM sodium phosphate 100 mM sodium chloride pH 7 buffer and protein concentrations were adjusted based on heme signal at 410 nm before size measurement.

Enzyme kinetics

To test the pH dependent peroxidase-like activity of DpsCytC chimeric cages, we compared the rate of oxidation of guaiacol and 3,3′,5,5′-tetramethylbenzidine substrates using rCytC as control. Free CytC (CytC_sigma) purchased as lyophilized powder was also tested as additional control. Purified proteins were dialyzed (×3) in 20 mM sodium phosphate 10 mM citrate combination buffer pH 4.25, 5.25, 6.25 and 7.25 respectively. Activity assays (8 wells at a time) were carried out at 25 °C using BioTek CYTATION5 imaging reader. Guaiacol stock solutions were prepared in buffer whereas TMB stock solutions were prepared in DMSO solvent. H_2O_2 and substrate stock solutions were prepared fresh every time before assay. 10 μL substrate (varying concentrations) was added to 96 well plate containing 186 μL enzyme and mixed quickly with pipetting, and the peroxidase reaction was initiated immediately by addition of 4 μL H_2O_2 (10 mM final concentration) to give a total reaction volume of 200 μL. The final enzyme concentration in all reactions was 0.5 μM, which was adjusted according to CytC monomer (extinction coefficient at 410 nm = 106 000 M^{-1} cm^{-1}).[33] H_2O_2 concentration determined at 240 nm (extinction coefficient 43.6 M^{-1} cm^{-1}).[34,35]

The rate of formation of guaiacol oxidation product (3,3′-dimethoxy-4,4′-biphenoquinone) was monitored every 10 seconds by increase in the absorbance at 470 nm (extinction coefficient 26 600 M^{-1} cm^{-1})[36,37] whereas TMB oxidation product (charge transfer complex) was also monitored every 10 seconds at 652 nm (extinction coefficient 39 000 M^{-1} cm^{-1}).[38] The activity assays were carried out three times (each in triplicate). Plots of the initial rates were corrected for any non-enzymatic background substrate oxidation and were fit to Michaelis–Menten kinetics model using Igor Pro 6.37.

Fluorescein-5-maleimide labelling

Dps-E158C mutant protein cages were used for site-specific fluorescein dye conjugation. Purified protein was buffer exchanged to Dulbecco's PBS (DPBS) buffer. Briefly, 1 mg mL^{-1} protein was incubated with ×100 excess DTT per subunit for 2 hours at room temperature. Dps-E158$C_{Reduced}$ protein cages were dialyzed twice (2 h each) in DPBS buffer to remove DTT and protein was concentrated using Amicon filter. Dps-E158$C_{Reduced}$ cages were resuspended in gently heated DPBS buffer pH 7.2 containing 8 M GuHCl to give 6 M GuHCl final concentration. Fluorescein-5-maleimide dye (F5M, in DMSO) was mixed at stoichiometric ration of 2 molar equivalent per subunit and reacted for 4 h at room temperature with gentle rocking. The conjugation reaction was quenched with β-mercapto ethanol (BME, 1 mM final concentration). The reaction mixture was then dialyzed (×3) to remove unreacted dye, BME and GuHCl and protein was further buffer exchanged by centrifugation using Amicon filters (×5) to remove any non-specific dye molecules sticking on Dps. Fluorescein labelling was confirmed by SDS-PAGE and mass spectrometry analysis and labelled cages were also characterized by TEM.

pH measurement inside Dps nanocages

Purified Dps-E158C-F5M cages were dialyzed (×2) into 20 mM Phosphate 10 mM Citrate buffer (pH 5.25–7.25); 20 mM Tris buffer for pH 7.75–8.75 buffer and 20 mM sodium bicarbonate buffer pH 9.25 respectively. pH dependent UV-Vis spectra for E158C-F5M were obtained. A similar pH dependent UV-Vis spectrum was obtained for free F5M dye by resuspending dye (10 μM final concentration) in buffer of desired pH (×1000 excess by volume). Absorbance at 490 nm (A_{490}) for the dianion (extinction coefficient 76 900 M^{-1} cm^{-1}) and absorbance at 453 nm (A_{453}) for the anion (extinction coefficient 29 000 M^{-1} cm^{-1}) was used to calculate concentration ratio of [dianion] to [anion] species respectively.[39] The ratio was used to get experimental pH values which were fitted using Henderson–Hasselbalch equation as ratio = $10^{\wedge(pH-pK_a)}$ to calculate pK_a for free and Dps labelled F5M dye using sigmoidal fit function in Igor pro.

SYPRO orange dye based thermal shift assay

All protein samples were buffer exchanged into 50 mM sodium phosphate 100 mM sodium chloride pH 7 and concentration were adjusted to 1 μM. Thermal shift assay was performed on StepOnePlus Real-Time PCR System (Applied Biosystems) using a previously reported procedure.[40] Sample preparation was done by adding 0.2 μL SYPRO Orange Protein Gel Stain (Sigma) to 250 uL protein sample. 25 μL assay mixture was analyzed with temperature elevating from 25 °C to 99.9 °C with a ramp rate of 1 °C per 2 min. The results of the assays were analyzed by Protein Thermal Shift Software (Thermo Fisher Scientific).

Results and discussion

Simultaneous proteins co-expression in the *E. coli* expression system to encapsulate CytC inside Dps

The self-assembly of chimeric Dps protein cages encapsulating heme bound CytC was achieved after simultaneous expression of three components in *E. coli* (Fig. 1). A 6His-Dps-CytC fusion protein and unmodified Dps subunit proteins were overexpressed in *E. coli* in the presence of co-transformed pEC86 plasmid which allowed constitutive expression of *ccm* genes (C-type cytochrome gene maturation) resulting in the *in-vivo* assembly of Dps-like cages. pEC86 plasmid is a derivative of pACYC184 plasmid that encodes for eight *ccm* genes (*ccmABCDEFGH*) that helps in heterologous C-type cytochrome heme binding and maturation under aerobic culture growth conditions.[41,42] The assembled Dps cages comprised a limited number of 6His-Dps-CytC subunits, due to cargo volume constraints, and a majority of unmodified Dps subunits. Chimeric cages differed from wild type assembled dodecameric Dps cages by presentation of a 6His tag on the exterior of the cage and encapsulation of CytC fused to Dps subunits on the interior of the cage.

When overexpressed alone, the 6His-Dps-CytC formed insoluble aggregates of the 36 kDa protein, suggesting that it failed to self-assemble into a dodecameric Dps-like cage structure. The expression of the 6His-Dps-CytC was confirmed by sodium-dodecyl sulphate polyacrylamide gel electrophoresis (SDS-PAGE) gel after cell lysis (Fig. S2, ESI†). Considering the size of the CytC and the volume of the Dps cage interior cavity a maximum 2 CytC enzymes could be encapsulated (Section S3, ESI†) suggesting this limitation of the available volume prevents correct assembly of the 6His-Dps-CytC into a dodecameric cage and resulted in the observed aggregation.

Purification and characterization of DpsCytC chimeric cages and free rCytC

When 6His-Dps-CytC was expressed together with unmodified Dps subunits, chimeric cages assembled and were purified by nickel affinity column chromatography using the polyhistidine tag, present only on the exterior of cages that also contained the Dps subunit fused to CytC (Fig. S3a, ESI†). The chromatogram showed a single elution peak, which exhibited both protein (280 nm) and heme (410 nm) spectroscopic signatures, confirming the heme association with the DpsCytC cages. Analysis of the purified protein by SDS-PAGE showed bands corresponding to 6His-Dps-CytC protein (36 kDa) and Dps protein (22 kDa) confirming their association in the purified chimeric DpsCytC cages (Fig. S3b, ESI†). Background impurity proteins were separated from DpsCytC chimeric cages by size exclusion chromatography (Fig. S3c, ESI†) and characterized by SDS-PAGE gel (Fig. 2a). The ratio of 6His-Dps-CytC to Dps peak areas obtained from densitometry analysis of the SDS-PAGE gel estimated 1 DpsCytC subunit per 11 Dps subunits, suggesting on average 1 CytC was encapsulated per cage (Fig. S3d, ESI†). Transmission electron microscopy (TEM) showed the formation of 9.7 ± 0.4 nm DpsCytC cages which were morphologically indistinguishable from the 9.5 ± 0.3 nm diameter dodecameric wild type Dps cage (Fig. 2b).

The average molecular weight of the DpsCytC chimeric cages, determined by size exclusion chromatography coupled with multi-angle light scattering (SEC-MALS), was observed to be 271.1 ± 1.1 kDa which is 9.1 ± 2.6 kDa larger than the empty Dps cage (262.0 ± 2.4 kDa) and consistent with encapsulation of a single 12 kDa CytC per Dps cage (Fig. 2c). UV-Vis spectroscopy of purified fractions also showed protein absorption at 280 nm and soret band absorption at 410 nm (Fig. S3e, ESI†), which was used to quantify heme bound to CytC. Analysis of protein and heme suggested that approximately 20% of the encapsulated CytC had heme incorporated, which is similar to observations reported in the literature for expression of other variants of CytC in *E. coli*.[43,44] Passive encapsulation of rCytC, by co-expressing it together with unmodified Dps and CytC maturation genes, resulted in negligible CytC encapsulation (Section S5 and Fig. S4, ESI†).

The free recombinant CytC protein (rCytC) was heterologously expressed in *E. coli*, co-transformed with the pEC86 plasmid, under similar expression and induction conditions used for DpsCytC chimeric cages. Purification by cation exchange showed a single major elution peak corresponding

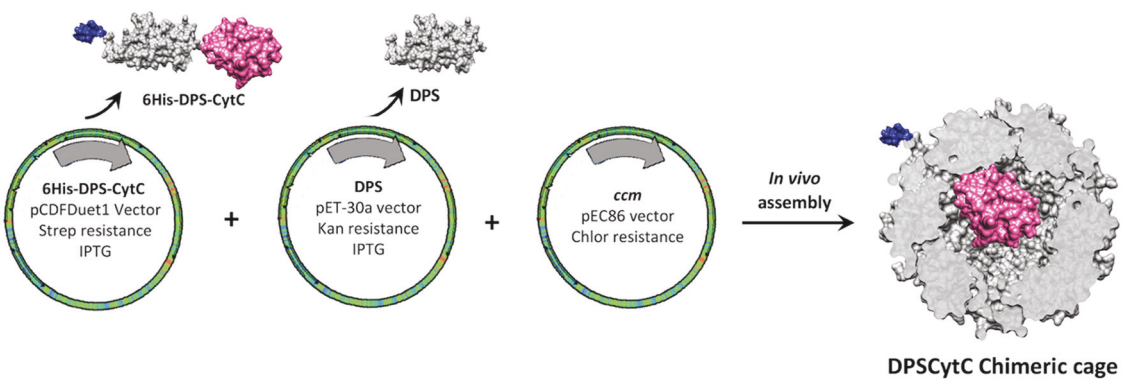

Fig. 1 Scheme showing three vector simultaneous expression, self-assembly, and encapsulation of CytC inside chimeric Dps cages. Dps subunits and 6His-Dps-CytC protein subunits were overexpressed in the presence of CytC maturation gene (*ccm* gene) to form DpsCytC chimeric cage encapsulating heme bound CytC inside and displaying polyhistidine tag on the exterior of the protein cage for selective purification of enzyme containing cages.

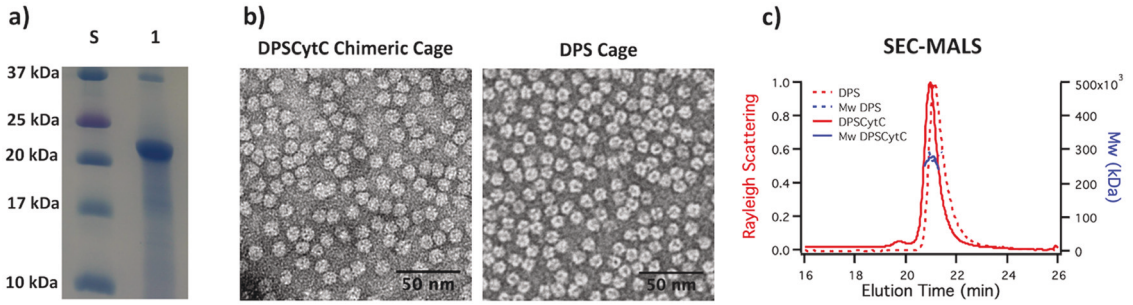

Fig. 2 Characterization of DpsCytC chimeric cages. (a) SDS-PAGE analysis showing the presence of both Dps and 6His-Dps-CytC protein subunit bands in purified chimeric cage sample (Lane 1), Lane S is standard protein ladder. (b) TEM micrographs showing DpsCytC chimeric cages (9.7 ± 0.4 nm) morphologically similar to wtDps cage (9.5 ± 0.3 nm). (c) SEC-MALS analysis showing Rayleigh scattering (red trace) and molar mass (blue trace) of DpsCytC chimeric cage as 271.1 ± 1.1 kDa corresponding to one CytC enzyme encapsulated per cage whereas molar mass of Dps cage (without cargo) was observed to be 262 ± 2.4 kDa, in comparison to 260 kDa the theoretical M_W of the Dps cage. DpsCytC cages eluted at 20.9 ± 0.1 min whereas Dps control cages eluted at 21.1 ± 0.1 min.

to rCytC (Fig. S5a, ESI†) with incorporated heme. Purified rCytC protein showed 12 kDa band on SDS-PAGE gel along with the presence of impurity bands (Fig. S5b, ESI†), which were separated by SEC purification and characterized by SDS-PAGE (Fig. S5c and d, ESI†). UV-Vis spectroscopy confirmed the presence of the heme peak at 410 nm in purified rCytC (Fig. S5e, ESI†). Mass spectrometry analysis of rCytC showed molecular weights corresponding to rCytC, with and without methionine (12 309 & 12 178 Da) and its acetylated form (12 221 Da) (Fig. S5f, ESI†).[45] This confirms that heme bound rCytC can be heterologously expressed in *E. coli* under aerobic growth conditions using simultaneous co-expression with CytC maturation genes.

Commercial CytC (Sigma-Aldrich, here after referred as CytC_sigma) was used as an additional free enzyme control. SDS-PAGE characterization of this material showed a single protein band corresponding to the expected molecular weight of 12.3 kDa for CytC (Fig. S7a, ESI†). Dynamic light scattering (DLS) analysis showed the hydrodynamic diameter of CytC to be 3.4 ± 0.1 nm which is consistent with the literature (Fig. S7b, ESI†).[26] UV-Vis spectroscopy also showed predominant peak at 410 nm corresponding to heme (Fig. S7c, ESI†). Mass spectrometry analysis of CytC_sigma showed molecular weight 42 Da higher than expected (Fig. S7d, ESI†) corresponding to acetylation of CytC at the N-terminus.[45]

Enzyme kinetics

Not all encapsulated CytC enzymes in the purified chimeric DpsCytC cages exhibited heme incorporation. Hence, the catalytic activity of DpsCytC chimeric cages and rCytC was tested by adjusting concentrations based on heme content. To assess the effect of encapsulation inside Dps on the peroxidase-like activity of CytC, catalytic activity was measured using two different substrates, 2-methoxyphenol (guaiacol) and 3,3′,5,5′-tetramethylbenzidine (TMB) for their oxidation in the presence of H_2O_2 between pH range 4.25–7.25. Dynamic light scattering (DLS) showed similar hydrodynamic diameter of DpsCytC chimeric cages under all kinetic assay conditions confirming the stability of the chimeric cages under these pH conditions (Fig. S8, ESI†). Free recombinant CytC, overexpressed under the same conditions, was used as a control (rCytC) and commercially available CytC (CytC_sigma) was used as additional unencapsulated control (Fig. S9, ESI†). The rate of guaiacol oxidation to form orange colored 3,3′-biphenoquinone was monitored at 470 nm and the TMB oxidation to form blue colored diamine/diamine charge transfer complex was monitored at 652 nm respectively (Fig. S10–S12, ESI†). The K_m, k_{cat}, and V_{max} of free and encapsulated CytC was obtained by fitting the data to a Michaelis–Menten model, where substrate inhibition was taken into consideration at high substrate concentrations.

pH dependent guaiacol oxidation kinetics

Chimeric DpsCytC cages showed guaiacol oxidation in a direct kinetic measurement confirming that the guaiacol substrate can diffuse into the chimeric Dps cages and react with the encapsulated CytC. The size of the guaiacol substrate (5.6 × 6.45 Å, Fig. S13, ESI†) is larger than Dps pores at either 3-fold axis (N-terminus ~ 3 Å, C-terminus ~ 4.2 Å, PDB 2CLB)[22] supporting previous hypothesis that the protein cage structure is likely dynamic in solution due to which the apparent pore size may differ slightly from the pore size obtained from structure determination.[46–51] DpsCytC showed consistently higher k_{cat} values at all four pH conditions tested when compared to the free rCytC control (Fig. 3, left panel). The trends in k_{cat} for both rCytC and CytC_sigma were similar with the exception of lower catalytic activity observed for CytC_sigma at pH 7.25 (Fig. S9, ESI† left panel). The DpsCytC showed lower substrate affinity (higher K_m) compared to free rCytC control. In general, the trend in pH dependent enzyme efficiency (k_{cat}/K_m) for both free rCytC and DpsCytC were similar (Fig. 3, left panel).

Catalytic activity differences between encapsulated and free enzymes were observed and to better understand this we plotted the kinetic data as the ratio of encapsulated to free rCytC. Upon encapsulation CytC showed high catalytic activity at all pH conditions when compared to free rCytC (Fig. 3, right panel). Encapsulated CytC showed 3 times higher turnover rates and 1.5 times higher efficiency at pH 5.25 compared to higher pH conditions (Fig. 3, right panel). K_m values for CytC upon encapsulation were similar at all pH conditions but higher than for the free rCytC. The difference in the catalytic

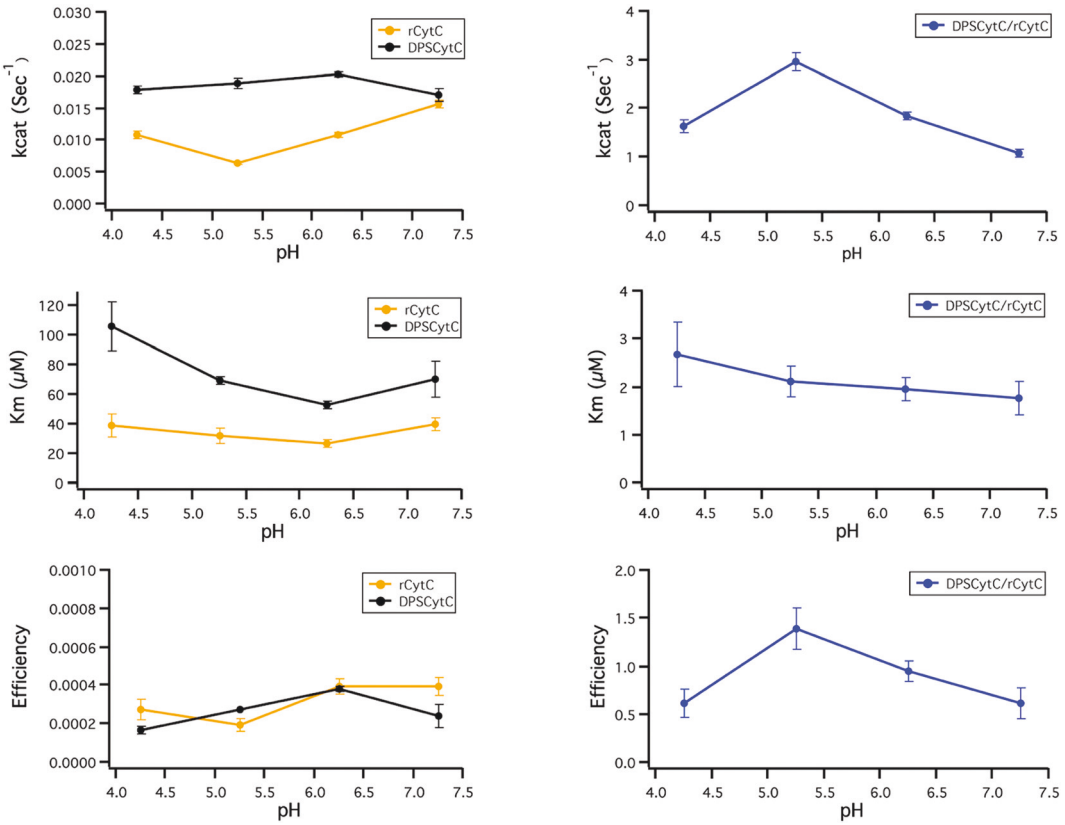

Fig. 3 pH dependent guaiacol peroxidase activity of free rCytC and CytC encapsulating Dps (DpsCytC). The panel on the left shows plots for k_{cat}, K_m and efficiency (k_{cat}/K_m) of DpsCytC (in black) and free rCytC enzyme (in orange) whereas the panel on right shows catalytic activity plotted as the ratios of the kinetic parameters of DpsCytC/rCytC to understand the effects due to enzyme encapsulation.

activity between encapsulated and free rCytC could be due to a number of potential reasons including (a) the high local concentration of enzyme inside Dps, (b) the unique microenvironment of the Dps cage interior or (c) pore effects.

Considering the interior volume of the Dps cage we estimate the local concentration of CytC inside Dps to be ~25 mM with 34% cargo packing density by volume, when an average of 1 CytC is encapsulated per cage (Section S3, ESI†). Such high local concentration of the peroxidase-like protein with high packing density could contribute to the differences observed in catalytic activity between free and encapsulated CytC. At high concentrations free enzymes tend to self-aggregate and lose activity and this can be mitigated by stabilization of enzyme at high molar confinement upon adsorption, immobilization or encapsulation.[9,52–57] Low surface coverage, protein denaturation due to unfolding, or improper orientation can lead to loss of enzyme activity during immobilization. However, compartmentalization can stabilize the cargo due to shell-cargo interactions, prevent self-aggregation, aggregation and favour multimeric subunits from dissociating due to high local concentrations. We studied the concentration dependent aggregation behavior of free CytC by monitoring particle size using dynamic light scattering technique. We observed (by DLS) that free CytC starts aggregating at or above 5 μM as evidenced by presence of multiple species in the DLS intensity plot (Fig. S14 and Table S3, ESI†) and by the longer time required for decay of the correlation signal suggesting sample polydispersity with increasing protein concentration. This threshold CytC concentration is well above the concentration of free CytC used in catalytic activity assay (0.5 μM) and well below the calculated local concentration of CytC inside Dps (25 mM). In the case of the DpsCytC, the high encapsulated concentration is achieved through encapsulation of a single enzyme thus removing the possibility of enzyme self-aggregation.

Chemical reactions under conditions of confinement can behave differently compared to their bulk counterparts because the interior of the cage can provide a unique reaction environment.[58,59] The Dps cage interior surface is lined with an abundance of Asp and Glu amino acid residues, the deprotonation of which is affected by the local pH inside Dps. We anticipate that the local microenvironment inside the Dps nanocage would have different pH compared to bulk pH which could contribute to the observed catalytic activity difference for free and encapsulated CytC. Results for probing local pH inside Dps are discussed later. The effects of a highly (negatively) charged polymer environments on the enhanced activity of CytC has been reported[33,60] and are consistent with our observation of enhanced activity of the encapsulated CytC in the negatively charged interior environment of the Dps cage.

Dps possess pores at its two different types of three-fold axes, *i.e.*, at the N-terminal and at C-terminal interface.[22] The N-terminal

pore is similar to 3-fold axis pores in ferritins. It is about 3 Å in size and has local positively charged surface potential on the exterior and negatively charged surface potential in the pore interior.[22,61] The N-terminal pore is occluded due to Tyr-139 side chains, whose rotation may modulate pore dimensions.[22] The C-terminal pore is unique in Dps cages and is lined with carboxylates from Glu-55 at the outside edge of the pore, carbonyls from Met-54 and Glu-55 and carboxylate from Glu-61 (from the pore interior) making it highly acidic. It has negatively charged surface potential around exterior and interior surface of the pore and measures about 4.2 Å halfway down the pore from Gly-58.[22] During its natural biological activity of iron oxide mineralization the Dps pores likely mediate the entry of metal cations, similar to ferritin, and in the context of our current research pore charge could play a role in small molecule substrate diffusion. Diffusion of charged small molecule substrate through pores have been previously studied in ferritin[61] and other protein cage systems.[62,63]

To access the CytC enzyme encapsulated inside Dps, the substrate must diffuse through the protein shell, presumably through pores at the 3-fold axes. The amino acid residues around the pore define the pore charge at a given pH and affect its electrostatic interaction with charged small molecule substrates. The measured K_m values (for guaiacol as substrate) for the encapsulated CytC were found to be higher than for the free rCytC (Fig. 3, right panel) but similar at all four pH conditions tested. This might suggest that the local guaiacol concentration inside Dps could be different (lower) than the bulk concentration, a consequence of inhibited substrate diffusion across the Dps protein shell. If substrate size was limiting its diffusion into Dps, then one would anticipate higher K_m values for the larger TMB substrate (discussed in following section) which was not observed in our experimental results. This suggests that size effects alone are not the primary effect. The pK_a of guaiacol is 9.9 and thus guaiacol is expected to be largely neutral, with very small residual negative charge, under the assay conditions. The pK_a of the side chain carboxyl functional group of glutamate lining 3-fold axis pores is $\sim$4.2 making the pore negatively charged under the experimental conditions and thus slightly repulsive to the guaiacol substrate. If the local pH inside Dps is different (higher) than bulk pH, then it can affect the protonation state of guaiacol inside Dps and affect enzyme activity. Considering the pH inside Dps is 1.2 units alkaline than bulk pH (details discussed later), the presence of a small population of partially ionized guaiacol inside Dps could contribute to the small differences observed in K_m of encapsulated CytC. Alternatively, due to the orientation of the enzyme inside Dps, it is possible that the access to enzymes active site is slightly altered due to encapsulation or surrounding local protein microenvironment which could also affect substrate binding and could cause the modest differences in behavior.

pH dependent 3,3′,5,5′-tetramethylbenzidine (TMB) oxidation kinetics

Reaction of the DpsCytC with TMB in the presence of hydrogen peroxide resulted in the formation of the characteristic blue colored diamine/diamine charge transfer complex as the single electron oxidation product. This confirmed that the TMB substrate (6.7 × 10.9 Å, Fig. S13, ESI†), which is larger in size than guaiacol, can also diffuse into the chimeric cages and react with the encapsulated CytC. The pH dependent catalytic activity of DpsCytC with TMB was either similar or higher compared to the rCytC control (Fig. 4, left panel ESI†). In general, the catalytic activity of DpsCytC was consistent across these experimental conditions and decreased negligibly with increased pH. The highest catalytic activity of both encapsulated and free rCytC samples was observed at pH 4.25 (Fig. 4, left panel). The DpsCytC also showed similar affinity (K_m) for the TMB substrate compared to rCytC control (Fig. 4, left panel), an observation in contrast to slightly higher K_m values observed for encapsulated CytC with guaiacol (Fig. 3). The catalytic efficiency (k_{cat}/K_m) for both DpsCytC and rCytC decreased with increasing pH (Fig. 4, left panel). Similar pH dependent catalytic turnover, K_m and efficiency trends were observed between free CytC controls with the exception that CytC_sigma showed slightly lower catalytic turnover compared to rCytC (Fig. S9, right panel ESI†).

To assess the effects of encapsulation on CytC activity, we plotted the kinetics data as a ratio of encapsulated to free rCytC (Fig. 4, right panel). Upon encapsulation in Dps, CytC showed similar to higher pH dependent catalytic turnover when compared to free rCytC (Fig. 4, right panel). At pH 4.25, the catalytic turnover ratio was 1 suggesting similar catalytic activity whereas higher catalytic turnover was observed at pH 5.25, an observation and trend similar to guaiacol substrate (Fig. 3 and 4 right panels). This observation also suggest that the optimum activity shifted from pH 4.25 for the free enzyme to pH 5.25 upon enzyme encapsulation inside Dps. The catalytic turnover decreased further with pH increase above 5.25. The substrate affinity (K_m) for CytC upon encapsulation were similar to free enzyme except pH 5.25 conditions. As discussed with guaiacol substrate, the differences in catalytic turnover between the encapsulated and free CytC could be attributed to high molar confinement of CytC enzyme (25 mM) encapsulated in Dps, the unique microenvironment provided by Dps nanocage interior, and/or pore effects.

Variation in bulk pH affects the dissociation equilibrium of charged amino acids, the effective surface charge of the protein and its interactions.[27] Polymer conjugated CytC (CytC-poly(methacrylic acid)) was reported to have high catalytic activity over broad pH range which was attributed to local charge microenvironments provided by the polymer.[33] Similar observations were reported for CytC-poly(acrylic acid) conjugate where presence of side chain carboxylates on polymer suppressed formation of negatively charged Fe(III)-peroxo intermediate (compound III) due to unfavorable electrostatic interactions.[60] The structure of the Dps cage (PDB 2CLB)[22] reveals the presence of a large number of surface exposed Asp and Glu residues in the interior cavity which at pH above the pK_a of side chain carboxyl group ($\sim$4) would be deprotonated. We hypothesize that presence of large number of carboxylates on the interior of the Dps acts in a manner similar to the observed poly(acrylic acid).

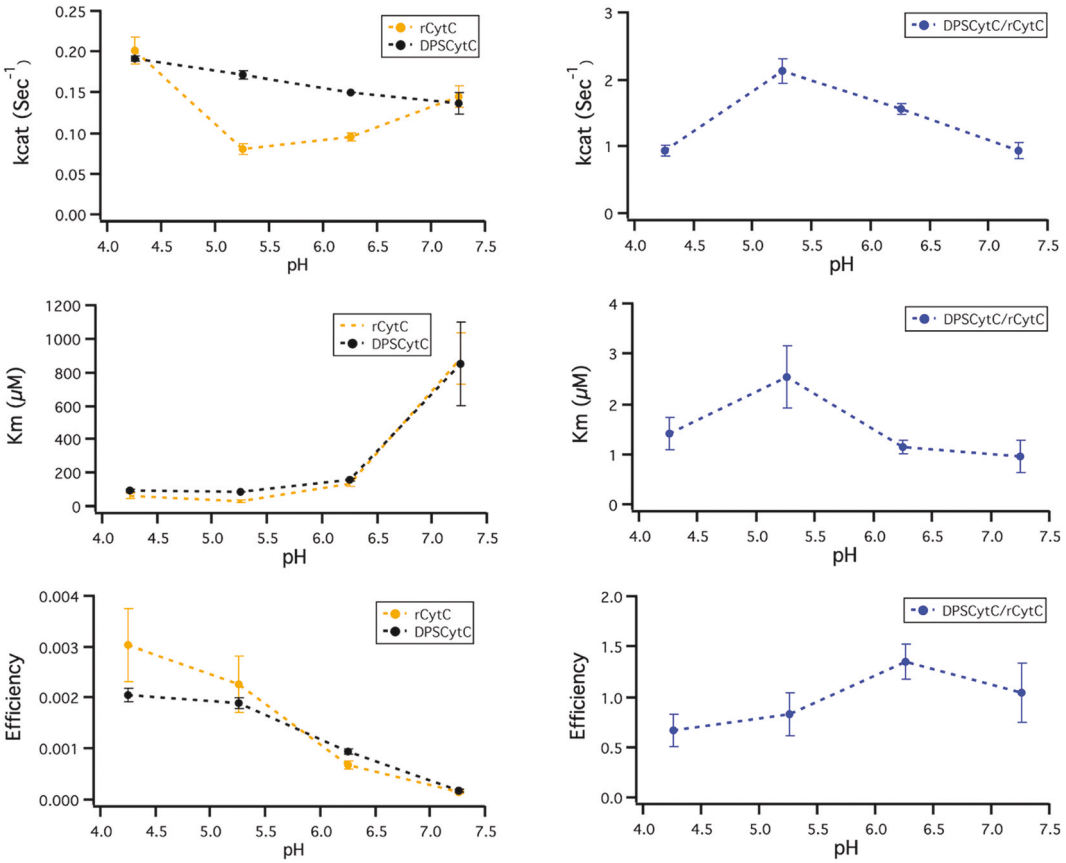

Fig. 4 pH dependent TMB peroxidase activity of free rCytC and Dps encapsulating CytC (DpsCytC). The panel on the left shows plots for k_{cat}, K_m and efficiency (k_{cat}/K_m) of DpsCytC (in black) and rCytC enzyme (in orange) whereas the panel on right shows catalytic activity plotted as the ratios of the kinetic parameters of DpsCytC/rCytC to understand the effects due to enzyme encapsulation.

The electrostatic interactions between Dps pore and substrate at a given pH could affect small molecule diffusion across the protein shell. The similar K_m values and K_m trends observed for TMB substrate for CytC upon encapsulation suggests that local TMB concentration inside and outside Dps are similar and TMB substrate diffusion into the Dps cage is not adversely affected by the protein barrier. The pK_a of the TMB substrate and the pK_a of carboxylate group of glutamates lining the C-terminal 3-fold axis pores are both ~4.2. This suggests that negative pore might allow the TMB substrate, which is neutral under the experimental conditions with small percentage of positively charged species, to transfer across the protein shell. This would establish roughly equal concentrations of TMB inside and in the bulk and contribute to the modest differences in K_m trends with TMB as substrate.

pH measurement inside Dps confinement

We used fluorescein dye as a pH sensitive indicator conjugated to the interior of Dps and compared its pH dependent behavior to free fluorescein in the bulk. Fluorescein dye exists in neutral, cation, anion and dianion forms depending on the pH in aqueous conditions with anion and dianion forms as the major species under slightly acidic to basic pH conditions (Fig. 5a).[39] Based on the structure of Dps, a reactive cysteine was engineered on the inside of the cage *via* a single point mutation (E158C). The Dps-E158C cage was chemically conjugated with fluorescein-5-maleimide (F5M) dye using standard thiol–maleimide coupling. SDS-PAGE gel (before Coomassie stain) showed Dps-F5M protein band in fluorescence confirming the fluorescein labelling and after Coomassie stain showed presence of protein band at the expected molecular weight (Fig. S15a, ESI†). TEM micrographs of the sample showed maintenance of Dps cage architecture after fluorescein labelling (Fig. S15b, ESI†). Fluorescein conjugation on Dps-E158C was also confirmed by mass spectrometry analysis which showed Dps subunit M_W corresponding to two fluorescein labelling per Dps subunit suggesting the engineered cysteine (E158C) (Fig. S15c and d, ESI†) as well as the endogenous cysteine present at position 135 which is generally buried, was also labeled with fluorescein. An 18 Da higher M_W observed per labeled fluorescein was observed, likely due to hydrolysis of maleimide to maleamic acid.[64]

The pH dependent absorbance of free fluorescein (F5M) and the Dps conjugate (Dps-F5M), was recorded between pH 5.25–9.25 (Fig. S16a and b ESI†). Analysis of this data, defined by single proton dissociation, was used to calculate pK_a's for the bulk and local (inside Dps) environment using the Henderson-Hasselbach equation. The speciation was measured by the absorbance spectroscopy for the anion (λ_{max} = 453 nm) and dianion

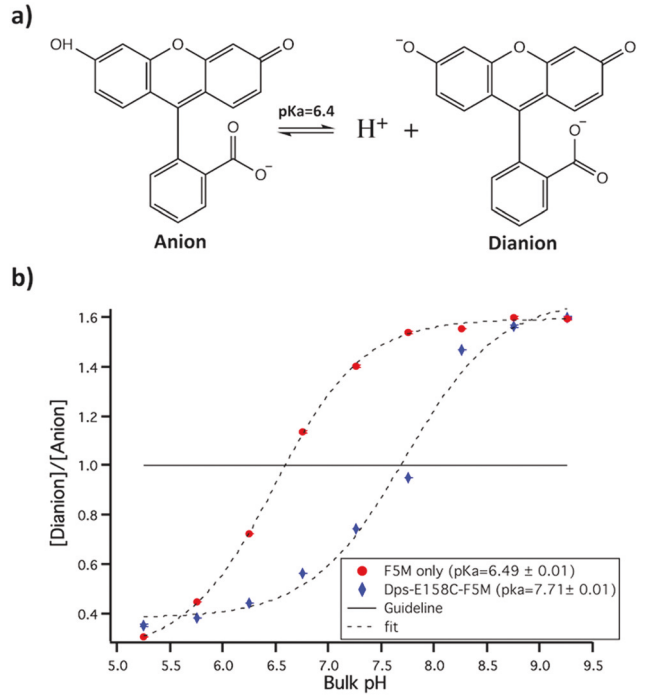

Fig. 5 (a) Scheme showing the acid dissociation of the pH sensitive dye fluorescein to form the anion and dianion forms. (b) The ratio of absorbance at 490 nm (dianion) and 453 nm (anion) at varying pH was used to determine the pK_a of free fluorescein-5-maleimide dye (F5M) and F5M conjugated at E158C residue of Dps interior cavity. A calculated pK_a of 6.49 ± 0.01 was obtained for free F5M dye whereas pK_a of 7.71 ± 0.01 was obtained for Dps-E158C-F5M cage suggesting local pH inside Dps is significantly different than bulk pH.

(λ_{max} = 490 nm) (Fig. S16c–e, ESI†). The ratio of [dianion] and [anion] was plotted against bulk pH and data were fit to determine the pK_a; the pH at which ratio was equal to 1 (Fig. 5b).

The calculated pK_a of the free dye was 6.49 ± 0.01, close to its reported value of 6.4, whereas the measured pK_a of Dps-Dye was found to be 7.71 ± 0.01. This result suggests the pH conditions under which analysis were made was above the pK_a of side chain carboxyl functional group of Glu/Asp and presumably they are deprotonated to form its conjugate base. This shift in pK_a by 1.2 pH units towards higher pH suggest that the conjugated dye inside the Dps is in local basic pH microenvironment compared to bulk solution. The presence of negatively charged carboxylate functional groups in Dps interior cavity could affect the acidity of hydroxyl functional group of conjugated fluorescein present in proximity, which now require higher [OH^-] to abstract proton from fluorescein thereby shifting the apparent pK_a to higher pH. Based on the experimental results and our hypothesis, we can conclude that local pH inside Dps is basic compared to bulk pH by ~1.2 pH units. Due to this, the pH optimum of CytC upon encapsulation shifted to pH 5.25 when ratio of turnover rates of DpsCytC:rCytC was taken into consideration for both guaiacol and TMB substrates.

Thermal stability assay

To study the thermal stability of CytC after encapsulation, a thermal shift assay was performed on DpsCytC chimeric cages, using free rCytC, CytC (Sigma) and empty Dps cage (lacking CytC) as controls. An increase in temperature resulted in denaturation and unfolding of protein with hydrophobic regions exposed, where SYPRO Orange dye selectively binds and resulting increase in fluorescence was recorded.[65] Thermal unfolding of free rCytC, CytC_sigma and empty Dps were observed at ~51, 52 and 65 °C respectively whereas the DpsCytC chimeric cage showed two a stage thermal denaturation at ~52 and 73 °C (Fig. S17, ESI†). A broad thermal denaturation at 52 °C for DpsCytC chimeric cage could be attributed to partial unfolding of encapsulated CytC compared to sharp transition observed for its free protein counterpart, suggesting that encapsulation limited thermal denaturation but did not significantly enhance the thermal stability of CytC. Interestingly, a second thermal denaturation at 73 °C observed for DpsCytC chimeric cage suggests an increase in Dps cage stability, possibly due to interaction between the Dps interior and the encapsulated CytC.

Conclusions

Here we have demonstrated a genetic approach for the self-assembly of DpsCytC chimeric cage nanomaterials using subcellular organelles as inspiration. We showed the successful formation of DpsCytC chimeric cages encapsulating active CytC with a peroxidase-like activity, through the simultaneous overexpression of 6His-Dps-CytC, unmodified Dps and *ccm* genes in *E. coli* system. Using the engineered polyhistidine tag on 6His-Dps-CytC subunit, we demonstrated selective purification of only enzyme containing chimeric cages using nickel-affinity column chromatography. Our results demonstrate that a single copy of the 3.4 nm diameter CytC is encapsulated inside the 5 nm interior cavity of Dps forming a 9 nm nanoreactor with high macromolecular confinement. This is a first example of protein-based enzyme encapsulation inside a Dps nanocage, which is possibly the smallest of all naturally occurring protein cage architectures. CytC encapsulated inside Dps showed better catalytic turnover compared to free enzyme control over broad pH range. The highest catalytic activity was observed at pH 5.25 while the free rCytC had an optimal activity at pH 4.25. This shift in pH optimum of encapsulated CytC was attributed to local pH microenvironment provided by Dps nanocage. Using fluorescein as pH sensor, we observed local pH inside Dps is ~1.2 units more basic compared to bulk pH conditions which could be the possible reason behind observed catalytic activity trends for encapsulated CytC. The DpsCytC chimeric nanoformulation has strong potential for utility and development as a targeted antioxidant therapeutic to mitigate oxidative stress.

Conflicts of interest

The authors declare no competing financial interest.

Acknowledgements

This work was supported by a grant from the National Science Foundation (NSF-NM CMMI-1922883). We thank the IU electron microscopy center, the IU Nanoscale Characterization Facility, the Physical Biochemistry Instrumentation Facility and the IU Biological Mass Spectrometry Facility for access to their instrumentation. The authors acknowledge the gift of plasmid pEC86 from Prof. Megan C. Thielges (Indiana University). The authors would also like to thank Ekaterina Selivanovitch and Yang Wang (Indiana University) for their valuable discussions.

Notes and references

1 A. J. Dzieciol and S. Mann, *Chem. Soc. Rev.*, 2012, **41**, 79–85.
2 M. Li, X. Huang, T. Y. Tang and S. Mann, *Curr. Opin. Chem. Biol.*, 2014, **22**, 1–11.
3 Y. M. Go and D. P. Jones, *Biochim. Biophys. Acta, Gen. Subj.*, 2008, **1780**, 1271–1290.
4 R. Docampo and S. N. J. Moreno, *Cell Calcium*, 2011, **50**, 113–119.
5 C. A. Kerfeld, S. Heinhorst and G. C. Cannon, *Annu. Rev. Microbiol.*, 2010, **64**, 391–408.
6 D. P. Patterson, B. Schwarz, R. S. Waters, T. Gedeon and T. Douglas, *ACS Chem. Biol.*, 2014, **9**, 359–365.
7 H. K. Waghwani, M. Uchida, C. Y. Fu, B. LaFrance, J. Sharma, K. McCoy and T. Douglas, *Biomacromolecules*, 2020, **21**, 2060–2072.
8 M. Comellas-Aragonès, H. Engelkamp, V. I. Claessen, N. A. Sommerdijk, A. E. Rowan, P. C. Christianen, J. C. Maan, B. J. Verduin, J. J. Cornelissen and R. J. Nolte, *Nat. Nanotechnol.*, 2007, **2**, 635–639.
9 S. Tetter and D. Hilvert, *Angew. Chem., Int. Ed.*, 2017, **56**, 14933–14936.
10 A. Macone, S. Masciarelli, F. Palombarini, D. Quaglio, A. Boffi, M. C. Trabuco, P. Baiocco, F. Fazi and A. Bonamore, *Sci. Rep.*, 2019, **9**, 11749.
11 R. J. Peters, M. Marguet, S. Marais, M. W. Fraaije, J. C. van Hest and S. Lecommandoux, *Angew. Chem., Int. Ed.*, 2014, **53**, 146–150.
12 L. Schoonen, R. J. Nolte and J. C. van Hest, *Nanoscale*, 2016, **8**, 14467–14472.
13 C. A. Kerfeld and O. Erbilgin, *Trends Microbiol.*, 2015, **23**, 22–34.
14 M. Sutter, D. Boehringer, S. Gutmann, S. Guenther, D. Prangishvili, M. J. Loessner, K. O. Stetter, E. Weber-Ban and N. Ban, *Nat. Struct. Mol. Biol.*, 2008, **15**, 939–947.
15 C. A. McHugh, J. Fontana, D. Nemecek, N. Q. Cheng, A. A. Aksyuk, J. B. Heymann, D. C. Winkler, A. S. Lam, J. S. Wall, A. C. Steven and E. Hoiczyk, *EMBO J.*, 2014, **33**, 1896–1911.
16 P. M. Harrison and P. Arosio, *Biochim. Biophys. Acta, Bioenerg.*, 1996, **1275**, 161–203.
17 M. Uchida, S. Kang, C. Reichhardt, K. Harlen and T. Douglas, *Biochim. Biophys. Acta, Gen. Subj.*, 2010, **1800**, 834–845.
18 S. Kang, L. M. Oltrogge, C. C. Broomell, L. O. Liepold, P. E. Prevelige, M. Young and T. Douglas, *J. Am. Chem. Soc.*, 2008, **130**, 16527–16529.
19 M. L. Ho, B. A. Adler, M. L. Torre, J. J. Silberg and J. Suh, *ACS Synth. Biol.*, 2013, **2**, 724–733.
20 M. L. Ho, J. Judd, B. E. Kuypers, M. Yamagami, F. F. Wong and J. Suh, *Cell. Mol. Bioeng.*, 2014, **7**, 334–343.
21 B. Wiedenheft, J. Mosolf, D. Willits, M. Yeager, K. A. Dryden, M. Young and T. Douglas, *Proc. Natl. Acad. Sci. U. S. A.*, 2005, **102**, 10551–10556.
22 G. H. Gauss, P. Benas, B. Wiedenheft, M. Young, T. Douglas and C. M. Lawrence, *Biochemistry*, 2006, **45**, 10815–10827.
23 W. S. Maaty, B. Wiedenheft, P. Tarlykov, N. Schaff, J. Heinemann, J. Robison-Cox, J. Valenzuela, A. Dougherty, P. Blum, C. M. Lawrence, T. Douglas, M. J. Young and B. Bothner, *PLoS One*, 2009, **4**, e6964.
24 M. Uchida, B. Maier, H. K. Waghwani, E. Selivanovitch, S. L. Pay, J. Avera, E. Yun, R. M. Sandoval, B. A. Molitoris, A. Zollman, T. Douglas and T. Hato, *J. Clin. Invest.*, 2019, **129**, 3941–3951.
25 M. O. Pereverzev, T. V. Vygodina, A. A. Konstantinov and V. P. Skulachev, *Biochem. Soc. Trans.*, 2003, **31**, 1312–1315.
26 N. Mirkin, J. Jaconcic, V. Stojanoff and A. Moreno, *Proteins*, 2008, **70**, 83–92.
27 R. J. Nap, A. L. Bozic, I. Szleifer and R. Podgornik, *Biophys. J.*, 2014, **107**, 1970–1979.
28 S. J. Maassen, P. van der Schoot and J. Cornelissen, *Small*, 2018, **14**, 7.
29 D. G. Bernard, S. Quevillon-Cheruel, S. Merchant, B. Guiard and P. P. Hamel, *J. Biol. Chem.*, 2005, **280**, 39852–39859.
30 Y. Y. Londer, *Methods Mol. Biol.*, 2011, **705**, 123–150.
31 C. C. Broomell, H. Birkedal, C. L. P. Oliveira, J. S. Pedersen, J. A. Gertenbach, M. Young and T. Douglas, *Soft Matter*, 2010, **6**, 3167–3171.
32 J. Schindelin, I. Arganda-Carreras, E. Frise, V. Kaynig, M. Longair, T. Pietzsch, S. Preibisch, C. Rueden, S. Saalfeld, B. Schmid, J. Y. Tinevez, D. J. White, V. Hartenstein, K. Eliceiri, P. Tomancak and A. Cardona, *Nat. Methods*, 2012, **9**, 676–682.
33 Y. F. Zhang, Q. Wang and H. Hess, *ACS Catal.*, 2017, **7**, 2047–2051.
34 K. Nazari, A. Mahmoudi, M. Shahrooz, R. Khodafarin and A. A. Moosavi-Movahedi, *J. Enzyme Inhib. Med. Chem.*, 2005, **20**, 285–292.
35 A. Mahmoudi, K. Nazari, M. Khosraneh, B. Mohajerani, V. Kelay and A. A. Moosavi-Movahedi, *Enzyme Microb. Technol.*, 2008, **43**, 329–335.
36 G. D. Depillis, B. P. Sishta, A. G. Mauk and P. R. O. Demontellano, *J. Biol. Chem.*, 1991, **266**, 19334–19341.
37 D. R. Doerge, R. L. Divi and M. I. Churchwell, *Anal. Biochem.*, 1997, **250**, 10–17.
38 P. D. Josephy, T. Eling and R. P. Mason, *J. Biol. Chem.*, 1982, **257**, 3669–3675.
39 R. Sjoback, J. Nygren and M. Kubista, *Spectrochim. Acta, Part A*, 1995, **51**, L7–L21.
40 Y. Wang, M. Uchida, H. K. Waghwani and T. Douglas, *ACS Synth. Biol.*, 2020, **9**, 3298–3310.
41 L. Thonymeyer, F. Fischer, P. Kunzler, D. Ritz and H. Hennecke, *J. Bacteriol.*, 1995, **177**, 4321–4326.

42 E. Arslan, H. Schulz, R. Zufferey, P. Kunzler and L. Thony-Meyer, *Biochem. Biophys. Res. Commun.*, 1998, **251**, 744–747.
43 Y. Y. Londer, P. R. Pokkuluri, D. M. Tiede and M. Schiffer, *Biochim. Biophys. Acta, Bioenerg.*, 2002, **1554**, 202–211.
44 E. H. J. Gordon, E. Steensma and S. J. Ferguson, *Biochem. Biophys. Res. Commun.*, 2001, **281**, 788–794.
45 T. Nakashima, H. Higa, H. Matsubara, A. M. Benson and K. T. Yasunobu, *J. Biol. Chem.*, 1966, **241**, 1166–1177.
46 D. W. Yang and K. Nagayama, *Biochem. J.*, 1995, **307**, 253–256.
47 H. Takagi, D. S. Shi, Y. Ha, N. M. Allewell and E. C. Theil, *J. Biol. Chem.*, 1998, **273**, 18685–18688.
48 G. C. Ford, P. M. Harrison, D. W. Rice, J. M. A. Smith, A. Treffry, J. L. White and J. Yariv, *Philos. Trans. R. Soc., B*, 1984, **304**, 551–565.
49 W. H. Massover, *Iron Biominer.*, 1991, 349–358.
50 F. Tama and C. L. Brooks, *J. Mol. Biol.*, 2002, **318**, 733–747.
51 L. O. Liepold, J. Revis, M. Allen, L. Oltrogge, M. Young and T. Douglas, *Phys. Biol.*, 2005, **2**, S166–S172.
52 D. M. Vriezema, M. C. Aragones, J. Elemans, J. Cornelissen, A. E. Rowan and R. J. M. Nolte, *Chem. Rev.*, 2005, **105**, 1445–1489.
53 H. J. Wagner, C. C. Capitain, K. Richter, M. Nessling and J. Mampel, *Eng. Life Sci.*, 2017, **17**, 36–46.
54 D. P. Patterson, B. Schwarz, K. El-Boubbou, J. van der Oost, P. E. Prevelige and T. Douglas, *Soft Matter*, 2012, **8**, 10158–10166.
55 U. Guzik, K. Hupert-Kocurek and D. Wojcieszynska, *Molecules*, 2014, **19**, 8995–9018.
56 Z. S. Aghamiri, M. Mohsennia and H. A. Rafiee-Pour, *Talanta*, 2018, **176**, 195–207.
57 J. Sharma and T. Douglas, *Nanoscale*, 2020, **12**, 336–346.
58 A. Kuchler, M. Yoshimoto, S. Luginbuhl, F. Mavelli and P. Walde, *Nat. Nanotechnol.*, 2016, **11**, 409–420.
59 J. P. Richard, T. L. Amyes, B. Goryanova and X. Zhai, *Curr. Opin. Chem. Biol.*, 2014, **21**, 1–10.
60 K. R. Benson, J. Gorecki, A. Nikiforov, W. Tsui, R. M. Kasi and C. V. Kumar, *Org. Biomol. Chem.*, 2019, **17**, 4043–4048.
61 T. Douglas and D. R. Ripoll, *Protein Sci.*, 1998, **7**, 1083–1091.
62 X. K. Yang, P. Arosio and N. D. Chasteen, *Biophys. J.*, 2000, **78**, 2049–2059.
63 J. E. Glasgow, M. A. Asensio, C. M. Jakobson, M. B. Francis and D. Tullman-Ercek, *ACS Synth. Biol.*, 2015, **4**, 1011–1019.
64 A. E. Boyatzis, S. D. Bringans, M. J. Piggott, M. N. Duong, R. J. Lipscombe and P. G. Arthur, *J. Proteome Res.*, 2017, **16**, 2004–2015.
65 K. Huynh and C. L. Partch, *Curr. Protoc. Protein Sci.*, 2015, **79**, 28.9.1–28.9.14.